Steam adsorption on molecular sieve 3A for sorption enhanced reaction processes

Jasper van Kampen[1,2] · Jurriaan Boon[1,2] · Martin van Sint Annaland[2]

Abstract

Steam adsorption enhanced reaction processes are a promising process intensification for many types of reactions, where water is formed as a byproduct. To assess the potential of these processes, adequate models are required that accurately describe water adsorption, particularly under the desired elevated temperatures and pressures. In this work, an adsorption isotherm is presented for H_2O adsorption at 200–350 °C and 0.05–4.5 bar partial pressure on molecular sieve (LTA) 3A. The isotherm has been developed on the basis of experimental data obtained from a thermogravimetric analysis and integrated breakthrough curves. The experimental data at lower steam partial pressures can be described with a Generalized Statistical Thermodynamic Adsorption (GSTA) isotherm, whereas at higher steam partial pressures the experimental data can be adequately captured by capillary condensation. Based on the characteristics of the adsorbent particles, a linear driving force relation has been derived for the adsorption mass transfer rate and the apparent micropore diffusivity is determined. The isotherm and mass transport model presented here prove to be adequate for modelling and improved evaluation of steam adsorption enhanced reaction processes.
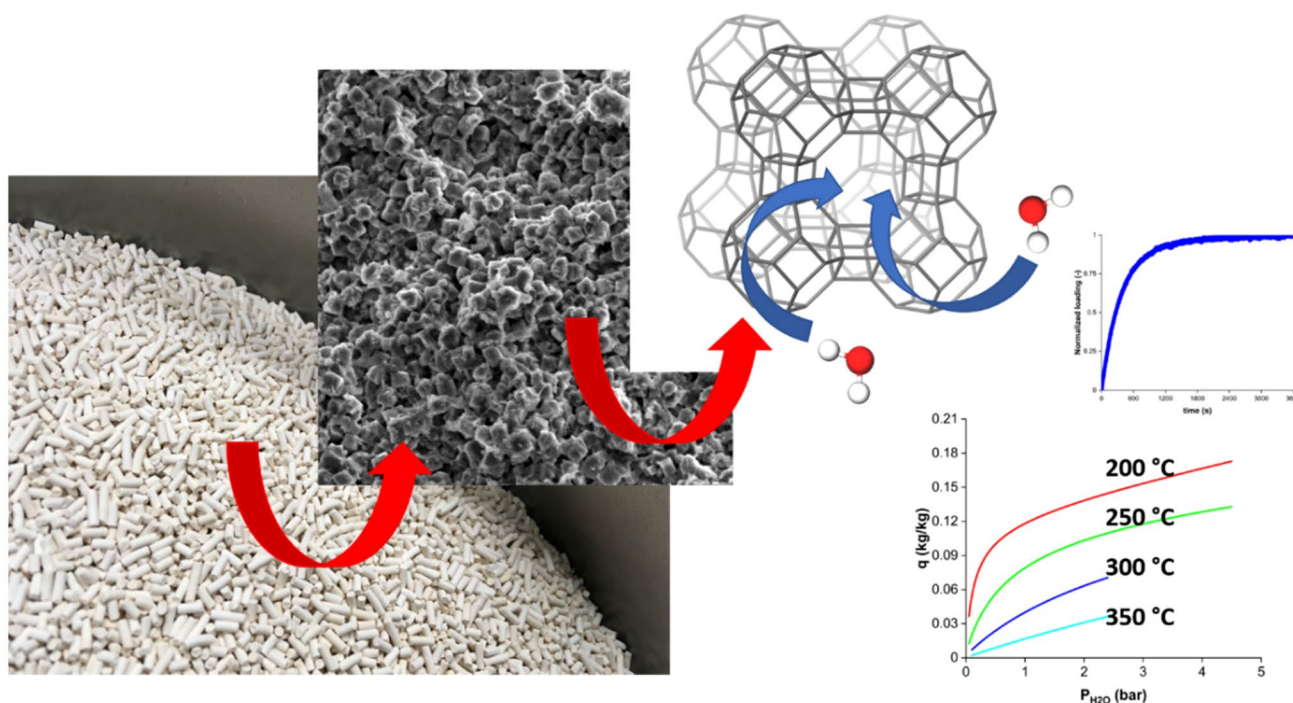
Extended author information available on the last page of the article

Springer

Nomenclature

a_p	Particle interfacial area (m² m⁻³)
b	Isotherm equilibrium constant (bar⁻¹)
d_c	Crystal diameter (m)
d_m	Macropore diameter (m)
d_p	Particle diameter (m)
D_c	Micropore diffusion coefficient (m² s⁻¹)
D_k	Knudsen diffusion coefficient (m² s⁻¹)
D_m	Molecular diffusion coefficient (m² s⁻¹)
D_p	Macropore diffusion coefficient (m² s⁻¹)
E_a	Activation energy (kJ mol⁻¹)
F_i	Molar flow of component i (mol s⁻¹)
k_f	External film mass transfer coefficient (m s⁻¹)
k_{LDF}	Linear driving force rate constant (s⁻¹)
K_L	Equilibrium constant of the multi-site Langmuir model
K_n	Equilibrium constant of the GSTA model (–)
m	Number of equilibrium parameters in the GSTA model
m_{ads}	Mass of adsorbent (kg)
M_i	Molecular weight of component i (kg mol⁻¹)
n	Index number of parameters and adsorption sites in the GSTA model
P	Pressure (bara)
P^0	Standard pressure (bara)
P_i	Partial pressure of component i (bara)
q_i	Adsorbent loading (mol kg⁻¹) or (kg kg⁻¹)
q_{max}	Maximum adsorption capacity (kg kg⁻¹)
q_s	Saturation capacity (kg kg⁻¹)
R	Ideal gas constant (J mol⁻¹ K⁻¹)
R_c	Crystal radius (m)
R_p	Particle radius (m)
Re	Reynolds number (–)
Sc	Schmidt number (–)
Sh	Sherwood number (–)
t	Time (s)
T	Temperature (K)
u	Superficial gas velocity (m s⁻¹)
v	Interstitial gas velocity (m s⁻¹)
V_g	Gas volume (m³)
y_i	Molar fraction of component i (–)

Greek Letters

γ	Surface tension (N m⁻¹)
ΔH^0	Standard molar enthalpy (kJ mol⁻¹)
ΔS^0	Standard molar entropy (J K⁻¹ mol⁻¹)
ε_b	Bed voidage (–)
ε_p	Particle porosity (–)
Λ	Partition function (–)
μ	Parameter corresponding to the adsorption potential (mol kg⁻¹) or (kg kg⁻¹)
ρ	Density (kg m⁻³)
ρ_p	Particle density (kg m⁻³)
τ	Tortuosity (–)

Abbreviations

DME	Dimethyl ether
GSTA	Generalized Statistical Thermodynamic Adsorption
LTA	Linde Type A
SEDMES	Sorption enhanced DME synthesis
SEM	Scanning electron microscopy
TGA	Thermogravimetric analysis

1 Introduction

Steam separation enhanced reaction processes show great potential as process intensification for many types of reactions, in which water is formed as a byproduct (van Kampen et al. 2019). Even so, the production and efficient handling of steam remains a major bottleneck for industrial CO₂ utilization (Centi and Perathoner 2009; Accelerating Breakthrough Innovation in Carbon Capture 2017; Katelhon et al. 2019). In this context, several groups have experimentally demonstrated the benefit of sorption enhancement in terms of product yield that exceeds the thermodynamic equilibrium in absence of steam adsorption (van Kampen et al. 2019,2020a; Kim et al. 2001; Carvill et al. 1996; Borgschulte et al. 2013; Ressler et al. 2006; Choi et al. 2002; Boon et al. 2019; Liuzzi et al. 2020). In parallel, modelling studies on sorption enhanced reactions have sought to conceptually understand sorption enhancement and focus on process design (van Kampen et al. 2020b; Iliuta et al. 2011; Parra et al. 2017,2018; Bayat et al. 2016; Guffanti et al. 2021). This work strongly relies on the understanding of the interaction of steam and the adsorbent under relevant conditions.

The majority of the experimental work on reactive steam adsorption uses Linde Type A (LTA) and Faujasite (Linde 13X) zeolite materials for water adsorption (van Kampen et al. 2019). Indeed, under the required operating conditions these materials show sufficient hydrothermal stability, possess adequate adsorption capacity, and adequate regeneration properties compared to other materials, such as typical chemisorbents (van Kampen et al. 2019; Kohl and Nielsen 1997). Where zeolites 13X, 5A and to lesser extent 4A are also used for CO₂ adsorption applications and potentially adsorb reaction products (Borgschulte et al. 2013; Walspurger et al. 2014; Terreni et al. 2019; Dirar and Loughlin

2013; Son et al. 2018; Sircar and Myers 2003; Lad and Makkawi 2014), zeolite 3A is highly selective for water due to size exclusion by its limited pore size (Fig. 1). Due to this high selectivity for water adsorption, zeolite 3A seems promising as adsorbent in sorption enhanced reactions for CO_2 conversion.

Extensive research has been carried out on the development, characterization and improvement of these materials for various applications (Sircar and Myers 2003; Ruthven 1984; Gren et al. 2010; Breck et al. 1956; Reed and Breck 1956). Although the heterogeneity of the adsorbent is often well described in a limited range by a semi-empirical isotherm correlation, such as the Sips and Toth isotherms (Kim et al. 2016; Gabruś et al. 2015), Llano-Restrepo et al. (2009) have shown that traditional adsorption models are not able to describe water vapor adsorption in zeolite 3A (Grace Davison) over a wide range of temperatures (−20 to 100 °C) and 8 orders of magnitude water vapor partial pressure (0.01 Pa up to 1 bar) (Llano-Restrepo and Mosquera 2009). They derived a Generalized Statistical Thermodynamic Adsorption (GSTA) model from Hill's statistical thermodynamic adsorption model, which is shown to be able to describe the water vapor adsorption correctly with seven statistical subsystems. With this model they provide a physical meaning to the statistical subsystems, so site specific (event) enthalpy and entropy could be obtained. In parallel to its thermodynamic derivation, the GSTA model can be seen as a multi-site Langmuir model in which the contribution to the capacity is equal for all sites (Ladshaw et al. 2015). The difference is in the energy attributed to a specific site for the heterogeneous Langmuir model compared to the energy attributed to the event of n molecules adsorbing for the GSTA model. In support of this, Wang (2020) recently showed that the same

dataset can be described by a triple-Langmuir model using the same number of fitting parameters (Wang 2020). Nonetheless, the adjustable number of equilibrium parameters makes the GSTA model flexible and capable of describing water adsorption (as well as other components) on molecular sieves (Ladshaw et al. 2015). However, the more parameters ($m + 2$ for the GSTA model) a model contains, typically the better the data description will be, as demonstrated by the recent results from Wang (2020).

In memory of Dr. Shivaji Sircar's extensive and groundbreaking work, we benefit from following it with respect to sorption enhanced reactions, adsorption equilibria, and mass transfer in adsorption. This article studies molecular sieve zeolite 3A under relevant conditions for the sorption enhanced CO_2 conversion by a combined experimental and modelling approach. Quantitative data for water adsorption at elevated temperature (200–350 °C) and partial pressure (0.05–4.5 bar) allows evaluation of a suitable adsorption isotherm under these conditions. Besides the adsorption capacity, the kinetics of adsorption are essential the for modelling and evaluation of applications of the adsorbent in sorption enhanced reaction processes (van Kampen et al. 2019; Sircar 2006). However, often the kinetics of adsorption is actually a mislabeling and the adsorbate mass transfer rate is measured and described (Sircar 2018). Therefore, a kinetic description of water adsorption is developed by means of a mass transfer rate model.

First, the material and its characterization for model parameter determination is reported, followed by the experimental procedure and model interpretation. The results and discussion section starts with the adsorption capacity and isotherm determination, followed by the kinetic description of water adsorption on zeolite 3A. Finally, the conclusions are summarized.

2 Materials and methods

2.1 Materials

Experiments were performed with molecular sieve type 3A, purchased as 1.6 mm pellets (UOP Molecular Sieves, Advanced Specialty Gas Equipment, USA), using the 1.6 mm pellets or a 212–425 μm sieve fraction. The material was analyzed by scanning electronic macroscopy (SEM) to determine the crystal and macropore size, which are used for the kinetic description of water adsorption on the material (Table 1). In Fig. 2 the cubical zeolite crystals can be clearly observed with an average (spherical) crystal diameter of 4 μm. Also, large macropores (1 μm) are present between the zeolite crystals.
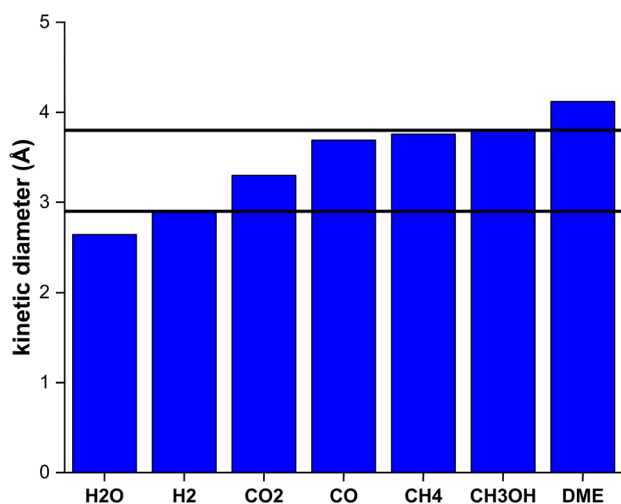

Fig. 1 Kinetic diameter of various components present in sorption enhanced reactions, compared to the pore sizes of zeolites 3A (2.9 Å) and 4A (3.8 Å) respectively (Sircar and Myers 2003; Ruthven 1984)

Table 1 Material parameters used for modelling

$q_{s,crystal}$ (wt.%)	25.5	Advanced Specialty Gas Equipment, New Jersey, USA
d_p (mm)	1.6	Advanced Specialty Gas Equipment, New Jersey, USA
ρ_b (kg m^{-3})	640	Advanced Specialty Gas Equipment, New Jersey, USA
ε_p (−)	0.662	Gabruś et al. (2015)
ε_b (−)	0.372	Gabruś et al. (2015)
d_m (µm)	1	This work
d_c (µm)	4	This work
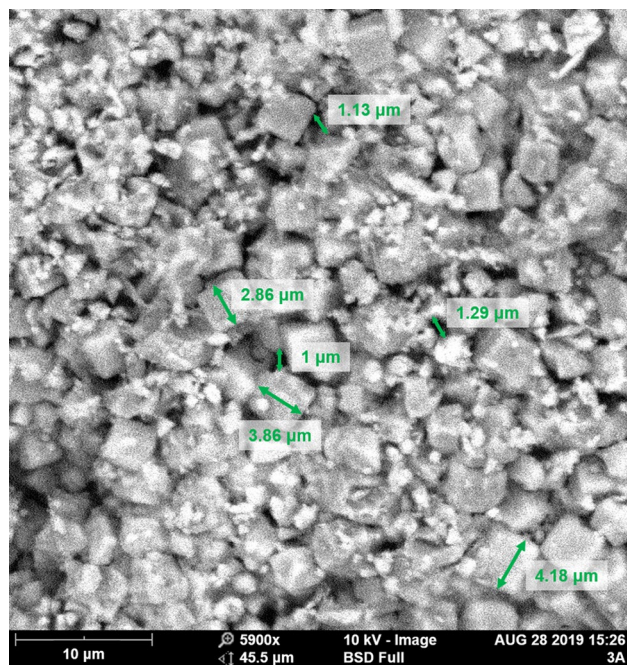
Fig. 2 SEM picture (5900x magnification) from cross-sectional cut of a 3A pellet with indicative sizes

2.2 Thermogravimetric analysis

Thermogravimetric analysis (TGA) was performed at the Eindhoven University of Technology (TU/e) on an in-house designed setup for operation up to 10 bar (HP-TGA, Fig. 3). A microbalance (Sartorius M25DD), with an operating range of 200 mg and a sensitivity of 1 µg, is used. The current experiments are performed in the range of 200–400 °C. A nitrogen stream is used to purge the balance and the reactor heating elements protecting them from contamination. The gas feeding system is equipped with Bronkhorst mass flow controllers (MFC) to produce different gas mixtures, and a Bronkhorst controlled evaporation mixing (CEM) system is installed to produce the desired quantities of steam with N$_2$ as carrier gas. All lines are traced and can be uniformly heated up to 450 °C to avoid steam condensation at elevated pressures. A porous ceramic basket was used with 50–100 mg of sample mass for each experiment. The gas flow rate was such that mass transfer

limitations due to the reduced volumetric flow rate in the reactor are avoided, which was verified by flow rate variation.

2.3 Breakthrough experiments

Experimental breakthrough runs were performed at TNO (Petten) on the 'Microflow 5' test-rig for atmospheric pressure experiments (Fig. 4). A quartz reactor with an internal diameter of 10 mm was filled with 2 g of sorbent resulting in a typical bed height of about 40 mm. During adsorption 100 ml$_N$ min^{-1} was fed to the reactor at 200–250 °C. The gas mixture contained 5–40 mol% H$_2$O, 5% CH$_4$ as tracer and balance N$_2$. Regeneration is performed by switching the gas flow to 100 mol% N$_2$, in some cases with increasing the temperature to 350 °C for 5 min. Off-gas analysis was performed continuously by a Perkin Elmer Frontier FTIR with heated Pike 2.4 m gas cell. After the experiment (regeneration step), the final mass of the sorbent is determined, and this value is used for the adsorption capacity calculations of each cycle. Experimental runs at high pressure were performed similarly, but were conducted on the high-pressure multi-column 'Spider' test-rig (Fig. 4). The reactors of 9.2 mm internal diameter, filled with 5 g sample, are electrically heated and can be run at pressure. During adsorption, the reactors were each fed with 150 ml$_N$ min^{-1} of gas mixtures at 200–250 °C and 5–30 bar(a) pressure. The gas mixtures consisted of 10–15 mol% water and 5 mol% argon as tracer in balance N$_2$. Adsorbent regeneration always consisted of periodically switching off the water supply, followed by decreasing the pressure. In some cases, the regeneration procedure included raising the temperature to 250–400 °C. Gas analysis was performed by a mass spectrometer (MS) measuring hydrogen (m/z = 2), water (m/z = 18), carbon monoxide/nitrogen (m/z = 28), argon (m/z = 40), and carbon dioxide (m/z = 44).

3 Data interpretation and model development

3.1 Data interpretation

In the TGA experiments a weight change is obtained, which can be used directly to study the cyclic sorption capacity. For
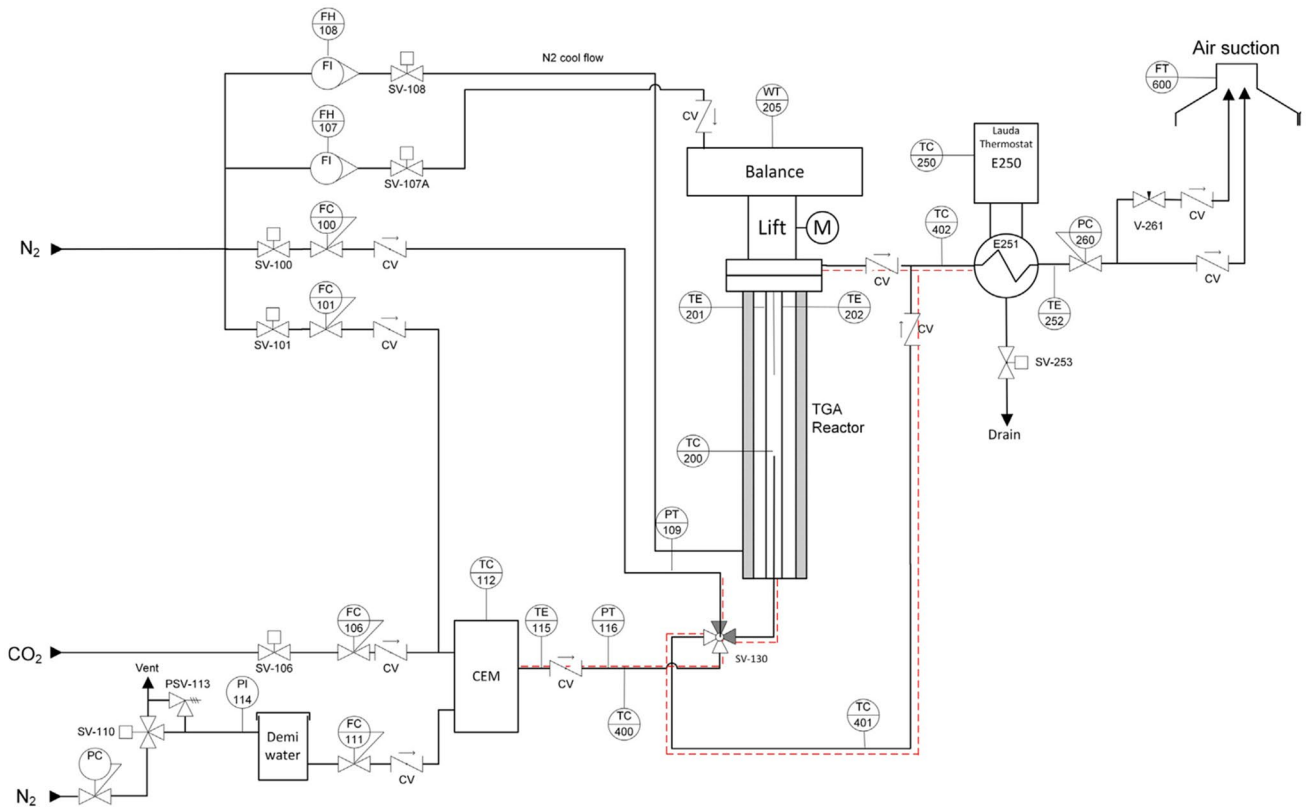
Fig. 3 P&ID of the HP-TGA setup

the breakthrough experiments, however, this is not the case. Setting up a material balance for component *i* over the reactor column, accumulation of component *i* between *t = 0* and complete breakthrough (*t = t_{end}*) must equal to the difference between the molar inflow and outflow rates.

$$\frac{y_i(t_{end})pV_g}{RT} + q_i(t_{end})m_{ads} - \frac{y_i(0)pV_g}{RT} - q_i(0)m_{ads} = t_{end}F_{i,in} - \int_{t=0}^{t_{end}} (y_iF)_{out}dt \tag{1}$$

The trapezoidal rule has been used for approximating the integral by a summation over discrete measurement data. The breakthrough of tracer ($q_{tracer} = 0$), prior to breakthrough of H_2O, is integrated to obtain V_g, the total interparticle and intraparticle gas volume, according to the Gibbsian surface excess concept (Sircar 2018; Talu 2011). After breakthrough, the tracer signal is used to quantify the outlet flow rate prior to and during breakthrough and Eq. 1 can then be used to compute the water loading (q).

In Fig. 5 an overlay of breakthrough experiments is shown. Both the breakthrough of tracer and water can be seen clearly. The comparable breakthrough signals also show that the experiments can be reproduced with significant accuracy. The cyclic stability of the material is confirmed, as shown in Fig. 6.

3.2 Model development

The adsorption capacity and mass transfer for water adsorption are determined by model evaluation. The material parameters used for modelling are reported in Table 1.

3.2.1 Adsorption isotherm model

Adsorption isotherms are derived on the basis of the underlying physics of sorbent-sorbate interaction. The GSTA model derived by Llano-Restrepo et al. is highly flexible in fitting *m* event energies and is given below (Llano-Restrepo and Mosquera 2009):

$$q = \frac{q_{max}}{m} \frac{\sum_{n=1}^{m} nK_n^0(\frac{P}{P^0})^n}{1 + \sum_{n=1}^{m} K_n^0(\frac{P}{P^0})^n} \tag{2}$$

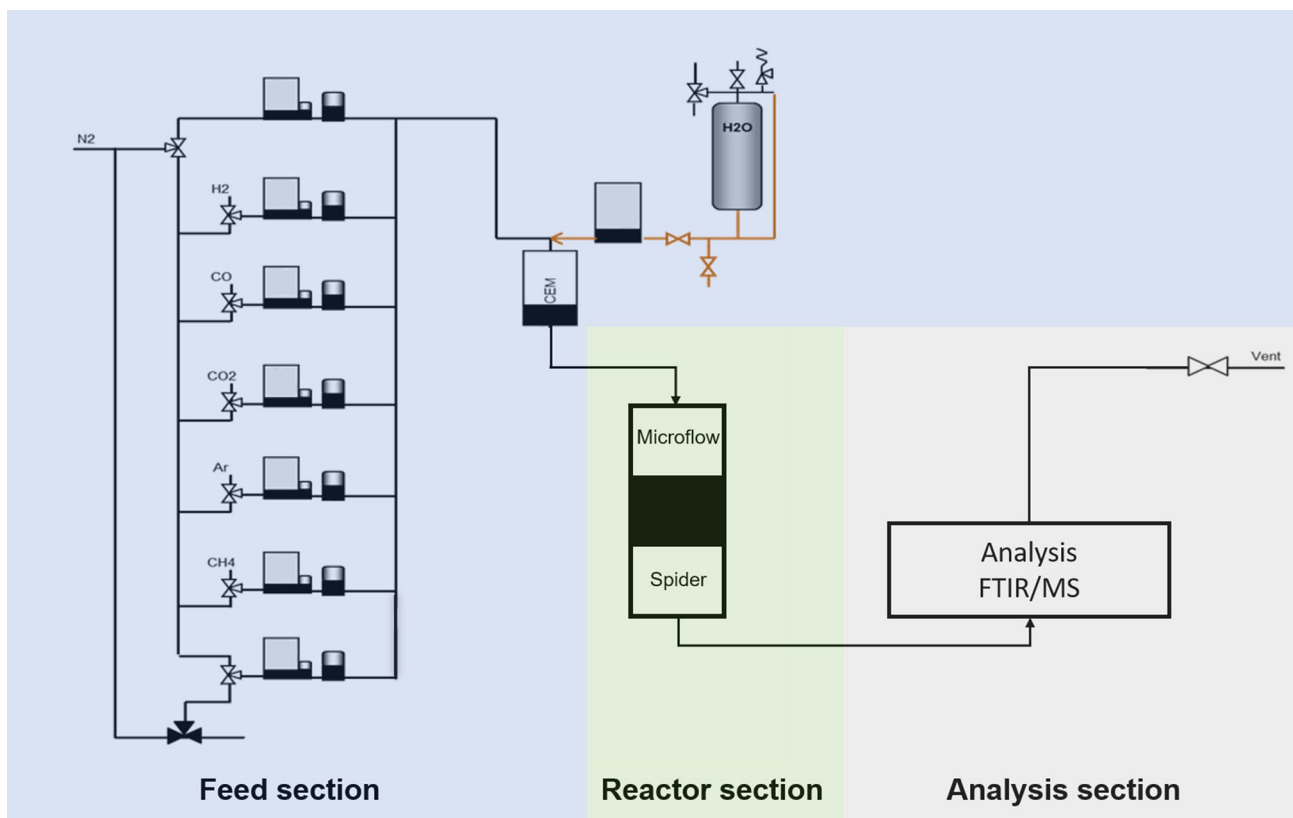$$\ln K_n^0 = -\frac{\Delta H_n^0}{RT} + \frac{\Delta S_n^0}{R} \tag{3}$$

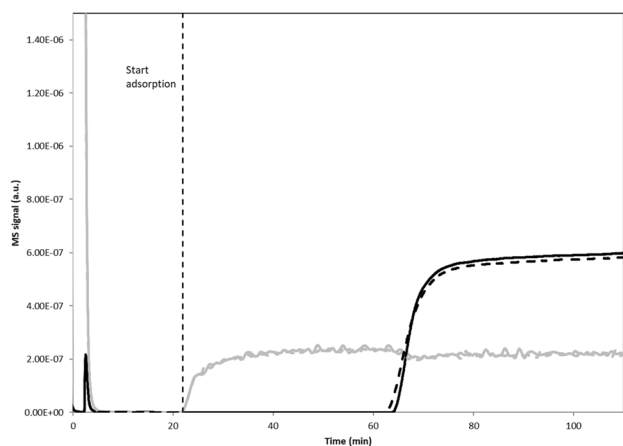**Fig. 4** Schematic presentation of the breakthrough testing units 'Microflow 5′' and 'Spider'

Fig. 5 Overlay of several breakthrough experiments with zeolite 3A at 250 °C adsorption temperature and 3 bar partial pressure: tracer signal (grey lines), H_2O cycle 55 (black solid line) and H_2O cycle 58 (black dashed line)
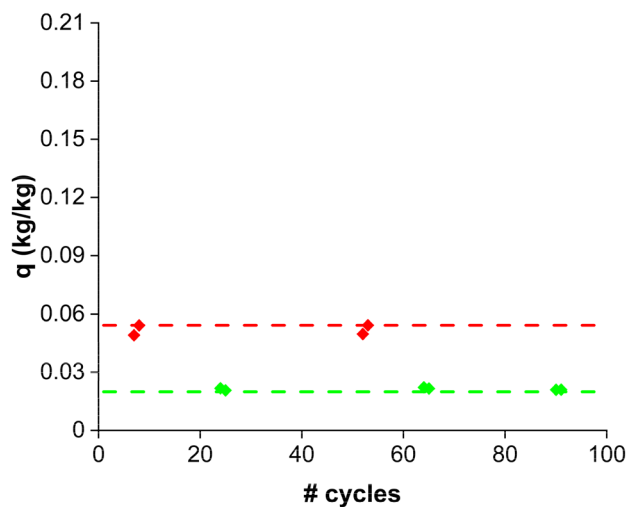

Fig. 6 Water loading observed during cyclic breakthrough experiments with zeolite 3A at 0.1 bar partial pressure and different temperatures (● (red) 200 °C, ● (green) 250 °C). Isotherm prediction is shown by the dashed lines

where q_{max} is the maximum (theoretical) adsorption capacity, m is the number of distinct adsorption sites (statistical subsystems), K^0_n is the dimensionless equilibrium constant with the standard-state pressure P^0 relative to the adsorption

of n molecules in a given statistical subsystem, and the standard enthalpy and entropy of these subsystems are represented by ΔH^0_n and ΔS^0_n. The model contains $m+2$ fitting

parameters, but in this work q_{max} is fixed as the maximum adsorption capacity given by the supplier.

As presented in the Introduction, the GSTA model can be seen as a special case of a multi-site Langmuir where the site contribution to the adsorption capacity is equal. The multi-site Langmuir model is given below:

$$q = \sum_{i=1}^{j} q_{s,i} \frac{K_{L,i}p}{1 + K_{L,i}p} \tag{4}$$

$$K_{L,i} = b_i e^{-E_{a,i}/RT} \tag{5}$$

here q_s is the saturation capacity of the specific site, j is the number of adsorption sites and K_L is the equilibrium constant of the Langmuir model. Each site has a different associated energy and is correlated with temperature according to the van't Hoff Eq. (5).

Capillary condensation describes the condensation of vapor into capillaries or small pores at vapor pressures lower than the saturation vapor pressure of the liquid with a planar surface (Butt et al. 2006). It is known to play a role in water adsorption on various porous adsorbents (Ruthven 1984) and can be described using the Kelvin equation, presented here for a sphere-like volume of radius r_{pore} (Butt et al. 2006):

$$\ln\left(\frac{p}{p_s}\right) = -\frac{2\gamma v_m}{RTr_{pore}} \tag{6}$$

where p_s is the saturation vapor pressure for a flat liquid surface, v_m is the molar volume of the liquid, γ is the surface tension and r_{pore} is the pore radius. Assuming the effective pore size is uniformly distributed (from 0 to r_{max}), one can derive the following equation (Liu et al. 2013):

$$q = \frac{\mu}{RTln(\frac{p_s}{p})} \tag{7}$$

$$\mu = \frac{2\gamma V_{pore}}{r_{max}} \tag{8}$$

In literature, between 2 and 7 (Gabruś et al. 2015; Llano-Restrepo and Mosquera 2009; Ladshaw et al. 2015; Wang 2020; Loughlin 2009; Lin et al. 2015) different energetic sites have been proposed for water adsorption on LTA zeolites. Clearly, the LTA framework consists of two distinct cavities which are accessible to water, the α and β cages (Breck et al. 1956; Reed and Breck 1956). It is shown that there are more adsorption sites, specifically related to the cation and its position in the α cage (Lin et al. 2015; Zhang et al. 2005). However, the energies found for the different sites by other authors are very close (Llano-Restrepo and Mosquera 2009; Ladshaw et al. 2015; Lin et al. 2015). Therefore, it is suggested here to consider three distinctive

sites. These sites correspond to the α cage and the β cage in the micropore and a mesopore contribution. Recently, a similar approach was used to describe water adsorption on zeolites 3A and 4A with a triple Langmuir isotherm (Wang 2020). It has been shown that a triple-site Langmuir is able to describe the water adsorption in zeolite 3A (Grace Davison) compared to the seven-site GSTA model (Llano-Restrepo and Mosquera 2009; Wang 2020). This can be explained by the fact that the authors use the same number of fitting parameters (9). However, it shows the validity of a multi-site Langmuir approach, of which the GSTA model is a special case. It does not explain the multilayer adsorption observed in this work and by other authors (Ruthven 1984; Kim et al. 2016; Ahn and Lee 2004), which does not occur in the micropores of the adsorbent, but rather in the mesopores (Ruthven 1984; Do 1998). Therefore, the third site could be described by a multilayer isotherm such as the generally used BET isotherm (Ruthven 1984; Do 1998; Aranovich and Donohue 1995). However, in a porous adsorbent multilayer formation will progress to capillary condensation, in which smaller pores are completely filled with water (Ruthven 1984). Taking this into account, the Kelvin equation can be used to describe multilayer formation and subsequent capillary condensation (Ruthven 1984; Liu et al. 2013; Ahn and Lee 2004; Sircar 1987; Sircar et al. 1996). Based on these considerations, a dual-site GSTA isotherm (Eq. 2 with $m=2$ or Eq. 4 with $j=2$ and $q_{s,i}=q_{s,j}$) plus the Kelvin equation (Eq. 7) are used to describe the water adsorption (Eq. 9):

$$q = \frac{fq_s}{m}\left(\frac{\sum_{n=1}^{m} nK_n^0(\frac{P}{P^0})^n}{1 + \sum_{n=1}^{m} K_n^0(\frac{P}{P^0})^n}\right) + \frac{\mu}{RTln(\frac{p_s}{p})} \tag{9}$$

The maximum capacity of the zeolite crystal is fixed at 25.5 wt.%, as given by the vendor and the pellet is considered to contain 20% binder (f=0.8) (Table 1).

3.2.2 Adsorption mass transfer model

In order to assess the adsorbate mass transport, the linear driving force (LDF) approximation is used (Sircar 2018; Glueckauf and Coates 1947; Glueckauf 1955). The overall mass transfer coefficient (k_{LDF}) can be defined as a series of resistances, consisting of external film resistance, macropore resistance, and micropore resistance, respectively (Ruthven 1984).

$$\frac{1}{k_{LDF}} = \frac{R_p\Lambda}{3k_f} + \frac{R_p^2\Lambda}{15\epsilon_p D_p} + \frac{R_c^2}{15D_c} \tag{10}$$

$$\Lambda = \epsilon_p + (1 - \epsilon_p)\rho_p \frac{\partial q}{\partial c} \tag{11}$$

The particle and crystal radius are given by R_p and R_c respectively. Similarly D_p and D_c are the macropore and micropore diffusivity. ε_p is the particle porosity and ρ_p its density. Λ is the partition ratio, describing the isotherm dependence. The film mass transfer coefficient (k_f) is estimated with the correlation by Wakao and Funazkri (Ruthven 1984):

$$Sh = 2 + 1.1 Re^{0.6} Sc^{1/3} \tag{12}$$

The equations used for the macropore and micropore diffusion are given in Table 2 (Ruthven 1984; Do 1998; Poling et al. 2001; Fuller et al. 1966).

4 Results and discussion

4.1 Adsorption capacity

Fig. 7 shows the equilibrium data for water vapor adsorption on the zeolite 3A. The breakthrough data align well with the TGA data at lower pressures, confirming the experimental approach. Where the TGA data start to deviate at higher steam partial pressures due to experimental uncertainty, the breakthrough data at higher pressures show an increasing adsorption capacity, as is known for this type of material at low temperatures (Ruthven 1984; Kim et al. 2016; Llano-Restrepo and Mosquera 2009; Lin et al. 2015).

In a porous adsorbent the observed multilayer formation will progress to capillary condensation (Ruthven 1984). Therefore, considering capillary condensation, a dual-site GSTA isotherm in combination with the Kelvin equation is used to describe the water adsorption (Eq. 9).
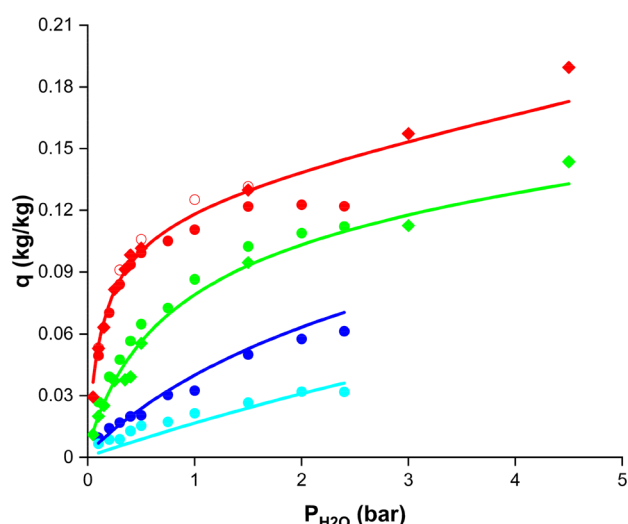

Fig. 7 Fit of the dual-site GSTA capillary condensation model to the adsorption isotherms data points of water vapor in zeolite 3A at different temperatures (● (red) 200 °C, ● (green) 250 °C, ● (blue) 300 °C, ● (cyan) 350 °C). Circles: experimental TGA data and crushed sample duplo (open circles); diamonds: experimental breakthrough data; solid lines: isotherm model with parameters from Table 3. Theoretical maximum capacity of the crystals is fixed at 25.5 wt.%

As is shown in Fig. 7 a good predictive quality is achieved for the experimental data. The resulting regressed parameters (Table 3) show two distinctive sites for the micropore adsorption.

Despite the different physical interpretation, it can be observed that the first event energy (attributed here to the α cage) aligns well with the values reported in literature, which are very close for subsequent events (Llano-Restrepo and Mosquera 2009; Ladshaw et al. 2015; Lin et al. 2015). The second event energy is significantly higher (less negative), which can be explained by the β cage contribution used here compared to the GSTA approach as used in literature. Whereas the GSTA model can be seen as a multi-site Langmuir isotherm with equal site contribution to the adsorption capacity (Ladshaw et al. 2015), the activation energies for the corresponding dual-site Langmuir can be determined. Although the experiments in this work are performed at elevated temperatures and pressures compared to previous works, the approximate energies found for the α and β cage, − 70 and − 10 kJ mol^{-1} respectively, are in agreement with the range reported in literature (Gabruś et al. 2015; Llano-Restrepo and Mosquera 2009; Ladshaw et al. 2015; Wang 2020; Loughlin 2009; Lin et al. 2015; Simo et al. 2009). Note that the contribution to the total capacity is considered equal, as for the GSTA model. Considering the smaller uptake in the β cage (1/3) compared to the α cage (2/3) (Lin et al. 2015), the activation energies become respectively 37% smaller and 10% larger.

**Table 2** Macropore and micropore diffusion equations

Macropore diffusivity	$D_p = \dfrac{\left(\frac{1}{D_m} + \frac{1}{D_K}\right)^{-1}}{\tau}$	Equation number 13
Molecular gas diffusivity	$D_{i,m} = \left(\displaystyle\sum_{\substack{j=1 \\ j \neq i}}^{n} \frac{x_j}{D_{i,j}}\right)^{-1}$	Equation number 14
Binary diffusion coefficients	$D_{AB} = \dfrac{0.00143 T^{1.75}}{P M_{AB}^{\frac{1}{2}} \left(\left(\Sigma_A \nu_i\right)^{\frac{1}{3}} + \left(\Sigma_B \nu_i\right)^{\frac{1}{3}}\right)^2}$	Equation number 15
Effective micropore diffusivity (Darken relation)	$D_c = D_c^* \dfrac{\partial \ln p}{\partial \ln q}$	Equation number 16
Micropore diffusivity	$D_c^* = D_c^0 e^{-E_a/RT}$	Equation number 17

Table 3 Parameters for the dual-site GSTA isotherm with capillary condensation on water adsorption data

Fixed parameters		Fitted parameters ± standard error			
q_s (kg kg^{-1})	0.255	ΔH^0_1 (kJ mol^{-1})	-62.4 ± 3.1	ΔS^0_1 (J K^{-1} mol^{-1})	-115 ± 5
f (–)	0.8	ΔH^0_2 (kJ mol^{-1})	-75.1 ± 31.0	ΔS^0_2 (J K^{-1} mol^{-1})	-160 ± 52
m (–)	2				

Table 4 Parameters for capillary condensation found for the dual-site GSTA (this work) and values found for capillary condensation on different types of alumina (Liu et al. 2013)

Temperature (K)	μ/RT (mol kg^{-1}) *This work*
473.15	2.63
523.15	1.67
573.15	0.849
623.15	0.196
Alumina	μ/RT (mol kg^{-1}) (Liu et al. 2013)
A1	0.975
AA300	5.76
Nakarai	5.44
F-200	9.57
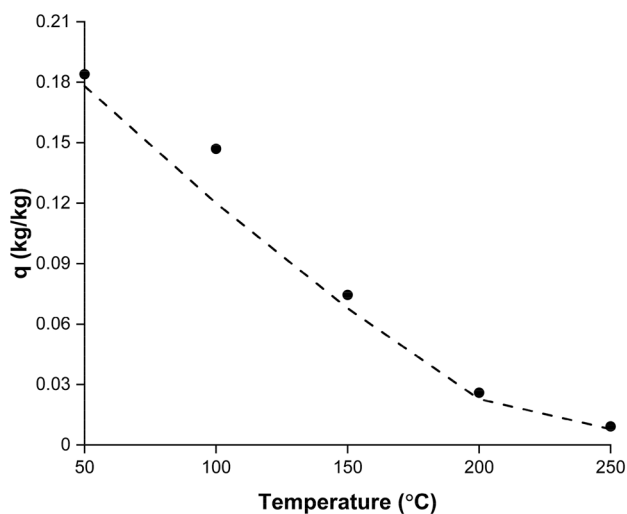
Fig. 8 GSTA model prediction (line) for low temperature data at a partial pressure of 2.337 kPa from Ghodhbene et al. (Ghodhbene et al. 2017)

The values found for capillary condensation are shown in Table 4. Taking the temperature dependence of the surface tension into consideration, the results are in the same order of magnitude with values reported in literature for alumina. The capillary condensation results also indicate that the condensation occurs in mesopores (20–500 Å) rather than actual larger macropores (> 500 Å), which is typical for capillary condensation (Butt et al. 2006). As shown in Fig. 8 the

model is able to describe low temperature data reported by other authors quite well, taking into account the model only uses two subsystems and capillary condensation (Ghodhbene et al. 2017). The capillary condensation, based on a uniform pore distribution, however, does not have a finite limit and cannot describe a type 4 isotherm of the Brunauer's classification fully. This will cause an overprediction at low temperature outside the scope of this work and a pressure close the saturation pressure, which could be solved by including the maximum amount adsorbed in the mesopore, if known (Liu et al. 2013, 2014). Despite the improvement which could be made for the region close to the saturation pressure, the isotherm model is able to describe the equilibrium data under sorption enhanced reaction temperatures and pressures well.

4.2 Adsorbate mass transfer

Besides the adsorption capacity at elevated temperatures, the kinetics of adsorption and the adsorbate mass transport are essential for the application of the adsorbent in a sorption enhanced reaction process (van Kampen et al. 2019; Sircar 2006). Figure 9 shows that the experimental mass transfer rate can be described well with the linear driving force (LDF) approximation (Glueckauf and Coates 1947; Glueckauf 1955), which can be explained by the parabolic concentration profiles in the adsorbent particle over long half-cycle times (Sircar and Hufton 2000a, b). This is observed for all partial pressures and temperatures (Fig. 9).

The overall mass transfer coefficient can be defined as a series of resistances (Eq. 10), contributed to by the external film resistance ($\frac{R_p \Lambda}{3k_f}$), macropore resistance ($\frac{R_p^2 \Lambda}{15\epsilon_p D_p}$) and micropore resistance ($\frac{R_c^2}{15D_c}$), respectively (Ruthven 1984; Sircar 2018). Other authors also confirmed the predictive capability of the LDF model for the water adsorption on zeolite 3A (Simo et al. 2009; Lin et al. 2014). The overall mass transfer resistance has been attributed to a combination of the external film resistance and the macropore resistance (Lin et al. 2014), or to a combination of the macropore and micropore resistances (Simo et al. 2009). If we calculate the external mass transfer resistance and the macropore resistance according to Eqs. 10–15, we observe that the data presented here are solely limited by the micropore resistance (Figs. 10, 11). Even if the macropore diameter would be a factor ten smaller (0.1 μm), the micropore resistance would make up more than 95% of the
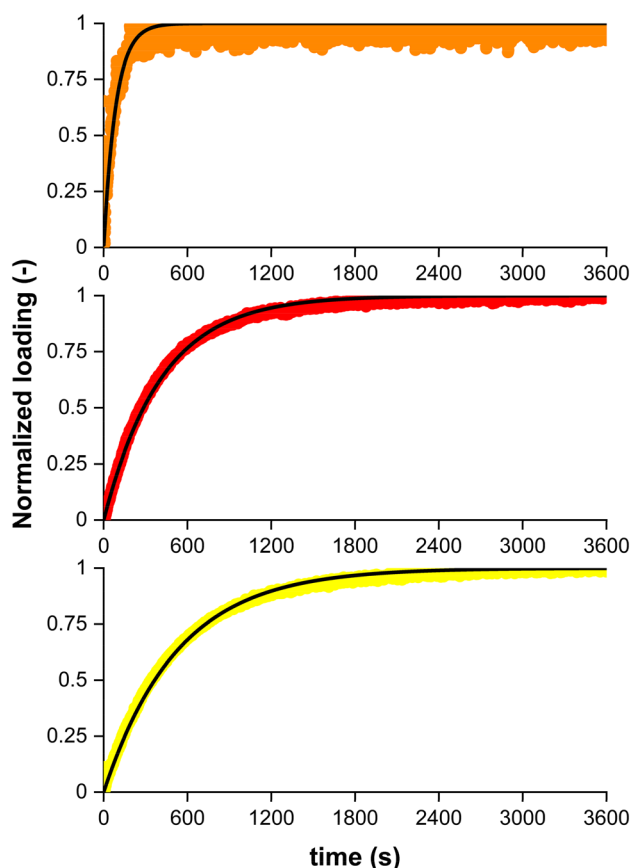
Fig. 9 Fit of LDF mass transfer rate (black lines) at 300 °C and 0.5 bar water partial pressure (top), 200 °C and 0.5 bar water partial pressure (middle) and 200 °C and 0.3 bar water partial pressure (bottom)

total mass transfer resistance. Also the practical adsorbent pellet size can vary, affecting the external film resistance and mainly the macropore resistance due to the quadratic dependence, which has been shown to influence the overall mass transfer coefficient significantly (Simo et al. 2009; Terreni et al. 2018). Experiments with varying pellet size would clarify the relative contribution of the different mass transfer resistances. In addition, direct imaging could be a powerful technique to circumvent possible issues arising from this, and is a good addition to the existing experimental methods (Terreni et al. 2018; Sircar 2007). As shown by the difference between the graphs in Fig. 9, the overall mass transfer coefficient increases with increasing partial pressure of water. Although the micropore resistance is always rate determining, the contribution of the micropore resistance to the overall mass transfer resistance increases with increasing partial pressure (Fig. 10). Despite the increasing micropore transfer rate at higher partial pressures, the decrease of the partition ratio (Eq. 11), and therefore the decrease in the macropore resistance, at higher partial pressures is larger. As expected, the increasing temperature also increases the overall mass transfer
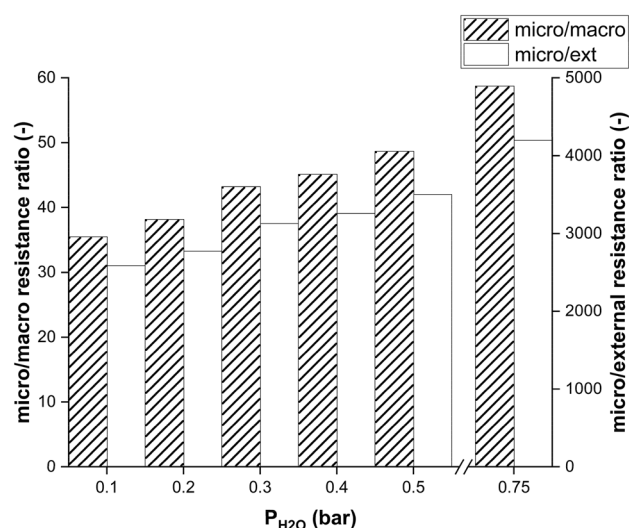

Fig. 10 Mass transfer resistances as ratio of the micropore resistance to the macropore resistance (left axis) and the external film resistance (right axis) for adsorption experiments at 200 °C

coefficient (Fig. 9). Although all diffusion mechanisms are temperature dependent and the diffusivities increase with increasing temperature, the partition ratio decreases with temperature since the adsorption is favored at low temperature. As a result there is a small decrease (98% to 97.3%) of the relative micropore resistance from 200 to 250 °C, and an increase (to 98.4%) going towards 350 °C (Fig. 11).

Knowing the respective contributions of the mass transfer resistances to the overall mass transfer coefficient, the micropore diffusivity can be calculated. Due to the small aperture of the micropores, the intracrystalline diffusion is relatively slow and the diffusivity is usually concentration and
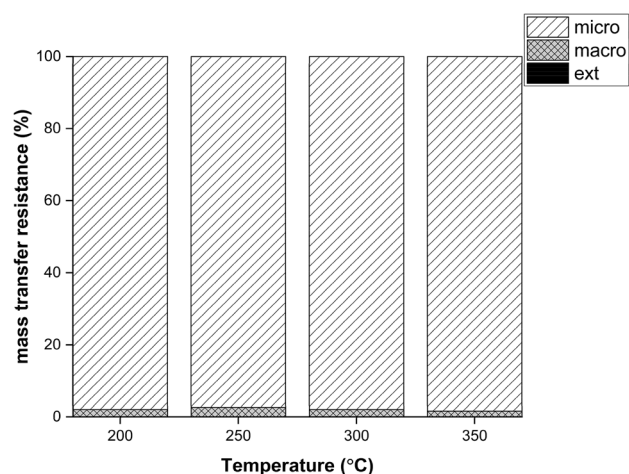

Fig. 11 Mass transfer resistances in percentage of overall resistance for adsorption experiments at 0.5 bar partial pressure

Table 5 Parameters for the micropore diffusivity (according to LDF model)

$D_c^0 (m^2 s^{-1})$	1.87×10^{-10}
E_a (kJ mol^{-1})	54.2

temperature dependent, given by the Darken relation (Eq. 16) (Ruthven 1984; Do 1998).

The values found for the micropore diffusivity are reported in Table 5. Relatively high indeed, the activation energy of 54.2 kJ mol^{-1} is in good agreement with values (of up to 60 kJ mol^{-1}) reported for zeolites A (Sircar and Myers 2003; Ruthven 1984; Simo et al. 2009). Clearly, the activation energy strongly depends on the sorbate diameter (Fig. 1) relative to the micropore size. Therefore, one could also expect a high activation energy for the small pore molecular sieve 3A.

As discussed for the adsorption capacity, there are multiple sites (α and β cage) for adsorption in zeolite 3A. Therefore multiple micropore diffusivities could be expected, in agreement with some authors who show a single LDF model not being able to predict the adsorption rate (Ghodhbene et al. 2017). Secondly, the LDF approximation is based on parabolic concentration profiles, which is known to be invalid for short cycle times (Alpay and Scott 1992; Carta 1993; Rodrigues and Dias 1998). Based on this a refinement of the current model could be made, but the experimental data show this is not required. Under the currently considered conditions, the adsorbate mass transfer described here proves to be significantly adequate for all modelling purposes. The LDF model has been verified experimentally for use in process modelling.

5 Conclusions

In conclusion, it is shown that molecular sieve (LTA) 3A has an adequate adsorption capacity at elevated temperatures, which increases rapidly at higher partial pressures of steam. This makes the LTA adsorbent suitable for sorption enhanced reaction processes, such as CO_2 conversion, enabling high yield condensation reaction products.

The water adsorption on the material can be described with a multi-site GSTA isotherm and additional capillary condensation. The multi-site isotherm can be best described as a dual-site GSTA isotherm (dual-Langmuir) corresponding to the respective α and β cages. Using a GSTA isotherm (or heterogeneous Langmuir) allows further flexibility in the number of distinct adsorption sites.

The adsorption mass transfer rate can be described by the linear driving force approximation, which is sufficiently accurate for all reactor and process modelling purposes. The mass transfer resistance during adsorption on zeolite 3A is shown to be dominantly determined by micropore resistance, due to the cage aperture.

Compliance with ethical standards

References

Accelerating Breakthrough Innovation in Carbon Capture, Utilization, and Storage, Report of the Mission Innovation Carbon Capture, Utilization, and Storage Expert's Workshop, 2017.

Ahn, H., Lee, C.-H.: Effects of capillary condensation on adsorption and thermal desorption dynamics of water in zeolite 13X and layered beds. Chem. Eng. Sci. **59**, 2727–2743 (2004)

Alpay, E., Scott, D.M.: The linear driving force model for fast-cycle adsorption and desorption in a spherical particle. Chem. Eng. Sci. **47**, 499–502 (1992)

Aranovich, G.L., Donohue, M.D.: A new approach to analysis of multilayer adsorption. J. Colloid Interface Sci. **173**, 515–520 (1995)

Bayat, M., Heravi, M., Rahimpour, M.R.: Sorption enhanced process by integrated heat-exchanger reactor assisted by fluidization concept for methanol synthesis. Chem. Eng. Process. **110**, 30–43 (2016)

Boon, J., van Kampen, J., Hoogendoorn, R., Tanase, S., van Berkel, F.P.F., van SintAnnaland, M.: Reversible deactivation of γ-alumina by steam in the gas-phase dehydration of methanol to dimethyl ether. Catal. Commun. **119**, 22–27 (2019)

Borgschulte, A., Gallandat, N., Probst, B., Suter, R., Callini, E., Ferri, D., Arroyo, Y., Erni, R., Geerlings, H., Züttel, A.: Sorption enhanced CO_2 methanation. Phys. Chem. Chem. Phys. **15**, 9620–9620 (2013)

Breck, D.W., Eversole, W.G., Milton, R.M., Reed, T.B., Thomas, T.L.: Crystalline zeolites I. The properties of a new synthetic zeolite, type A. J. Am. Chem. Soc. **78**, 5963–5971 (1956)

Butt, H.-J., Graf, K., Kappl, M.: Physics and Chemistry of Interfaces, 2nd edn. Wiley, Weinheim (2006)

Carta, G.: The linear driving force approximation for cyclic mass transfer in spherical particles. Chem. Eng. Sci. **48**, 622–625 (1993)

Carvill, B.T., Hufton, J.R., Anand, M., Sircar, S.: Sorption-enhanced reaction process. AIChE J. **42**, 2765–2772 (1996)

Centi, G., Perathoner, S.: Opportunities and prospects in the chemical recycling of carbon dioxide to fuels. Catal. Today **148**, 191–205 (2009)

Choi, J.-C., He, L.-N., Yasuda, H., Sakakura, T.: Selective and high yield synthesis of dimethyl carbonate directly from carbon dioxide and methanol. Green Chem. **4**, 230–234 (2002)

Dirar, Q.H., Loughlin, K.F.: Intrinsic adsorption properties of CO_2 on 5A and 13X zeolite. Adsorption **19**, 1149–1163 (2013)

Do, D.D.: Adsorption Analysis: Equilibria and Kinetics. Imperial College Press, London (1998)

Fuller, E.N., Schettler, P.D., Giddings, J.C.: A new method for prediction of binary gas-phase diffusion coefficients. Ind. Eng. Chem. **58**, 19–27 (1966)

Gabruś, E., Nastaj, J., Tabero, P., Aleksandrzak, T.: Experimental studies on 3A and 4A zeolite molecular sieves regeneration in TSA process: aliphatic alcohols dewatering-water desorption. Chem. Eng. J. **259**, 232–242 (2015)

Ghodhbene, M., Bougie, F., Fongarland, P., Iliuta, M.C.: Hydrophilic zeolite sorbents for in-situ water removal in high temperature processes. Can. J. Chem. Eng. **95**, 1842–1849 (2017)

Glueckauf, E.: Theory of chromatography Part 10: Formulae for diffusion into spheres and their application to chromatography. Trans. Faraday Soc. **51**, 1540–1551 (1955)

Glueckauf, E., Coates, J.I.: Theory of chromatography Part IV: The influence of incomplete equilibrium on the front boundary of chromatograms and on the effectiveness of separation. J. Chem. Soc. **1947**, 1315–1321 (1947)

Gren, W., Parker, S.C., Slater, B., Lewis, D.W.: Structure of zeolite A (LTA) surfaces and the zeolite A/water interface. J. Phys. Chem. C **114**, 9739–9747 (2010)

Guffanti, S., Visconti, C.G., van Kampen, J., Boon, J., Groppi, G.: Reactor modelling and design for sorption enhanced dimethyl ether synthesis. Chem. Eng. J. **404**, 126573 (2021)

Iliuta, I., Iliuta, M.C., Larachi, F.: Sorption-enhanced dimethyl ether synthesis: multiscale reactor modeling. Chem. Eng. Sci. **66**, 2241–2251 (2011)

Katelhon, A., Meys, R., Deutz, S., Suh, S., Bardow, A.: Climate change mitigation potential of carbon capture and utilization in the chemical industry. Proc. Natl. Acad. Sci. USA **116**, 11187–11194 (2019)

Kim, K.-M., Oh, H.-T., Lim, S.-J., Ho, K., Park, Y., Lee, C.-H.: Adsorption equilibria of water vapor on zeolite 3A, zeolite 13X, and dealuminated Y zeolite. J. Chem. Eng. Data **61**, 1547–1554 (2016)

Kim, H.-J., Jung, H., Lee, K.-Y.: Effect of water on liquid phase DME synthesis from syngas over hybrid catalysts composed of Cu/ZnO/Al_2O_3 and γ-Al_2O_3. Korean J. Chem. Eng. **18**, 838–841 (2001)

Kohl, A., Nielsen, R.: Gas Dehydration and Purification by Adsorption, Gas Purification. Gulf Publishing Company, Houston (1997)

Lad, J.B., Makkawi, Y.T.: Adsorption of dimethyl ether (DME) on zeolite molecular sieves. Chem. Eng. J. **256**, 335–346 (2014)

Ladshaw, A., Yiacoumi, S., Tsouris, C., DePaoli, D.: Generalized gas–solid adsorption modeling: single-component equilibria. Fluid Phase Equilib. **388**, 169–181 (2015)

Lin, R., Ladshaw, A., Nan, Y., Liu, J., Yiacoumi, S., Tsouris, C., DePaoli, D.W., Tavlarides, L.L.: Isotherms for water adsorption on molecular sieve 3A: Influence of cation composition. Ind. Eng. Chem. Res. **54**, 10442–10448 (2015)

Lin, R., Liu, J., Nan, Y., DePaoli, D.W., Tavlarides, L.L.: Kinetics of water vapor adsorption on single-layer molecular sieve 3A: experiments and modeling. Ind. Eng. Chem. Res. **53**, 16015–16024 (2014)

Liuzzi, D., Peinado, C., Peña, M.A., van Kampen, J., Boon, J., Rojas, S.: Increasing dimethyl ether production from biomass-derived syngas via sorption enhanced dimethyl ether synthesis. Sustain. Energy Fuels **4**, 5674 (2020). https://doi.org/10.1039/D0SE01172J

Liu, X.J., Shi, Y.F., Kalbassi, M.A., Underwood, R., Liu, Y.S.: Water vapor adsorption isotherm expressions based on capillary condensation. Sep. Purif. Technol. **116**, 95–100 (2013)

Liu, X.J., Shi, Y.F., Kalbassi, M.A., Underwood, R., Liu, Y.S.: A comprehensive description of water vapor equilibriums on alumina F-200: adsorption, desorption, and H_2O/CO_2 binary adsorption. Sep. Purif. Technol. **133**, 276–281 (2014)

Llano-Restrepo, M., Mosquera, M.A.: Accurate correlation, thermochemistry, and structural interpretation of equilibrium adsorption isotherms of water vapor in zeolite 3A by means of a generalized statistical thermodynamic adsorption model. Fluid Phase Equilib. **283**, 73–88 (2009)

Loughlin, K.F.: Water isotherm models for 4A (NaA) zeolite. Adsorption **15**, 337–353 (2009)

Advanced Specialty Gas Equipment, New Jersey, USA

Parra, A.A.M., Asmanoglo, C., Agar, D.W.: Cyclic steady-state behavior of a fixed-bed adsorptive reactor for reverse water-gas shift reaction. Chem. Eng. Technol. **40**, 915–926 (2017)

Parra, A.A.M., Asmanoglo, C., Agar, D.W.: Modelling and optimization of a moving-bed adsorptive reactor for the reverse water-gas shift reaction. Comput. Chem. Eng. **109**, 203–215 (2018)

Poling, B.E., Prausnitz, J.M., O'Connell, J.P.: The Properties of Gases and Liquids. McGraw-Hill, New York (2001)

Reed, T.B., Breck, D.W.: Crystalline zeolites II .Crystal structure synthetic zeolite, type A. J. Am. Chem. Soc. **78**, 5972–5977 (1956)

Ressler, S., Elsner, M., Dittrich, C., Agar, D., Geisler, S., Hinrichsen, O.: Reactive gas adsorption, Integrated Reaction and separation operations. Springer, New York (2006)

Rodrigues, A.E., Dias, M.M.: Linear driving force approximation in cyclic adsorption processes: simple results from system dynamics based on frequency response analysis. Chem. Eng. Process. **37**, 489–502 (1998)

Ruthven, D.M.: Principles of Adsorption and Adsorption Processes. Wiley, New York (1984)

Simo, M., Sivashanmugam, S., Brown, C.J., Hlavacek, V.: Adsorption/desorption of water and ethanol on 3A zeolite in near-adiabatic fixed bed. Ind. Eng. Chem. Res. **48**, 9247–9260 (2009)

Sircar, S.: Basic research needs for design of adsorptive gas separation processes. Ind. Eng. Chem. Res. **45**, 5435–5448 (2006)

Sircar, S.: Recent developments in macroscopic measurement of multicomponent gas adsorption equilibria, kinetics, and heats. Ind. Eng. Chem. Res. **46**, 2917–2927 (2007)

Sircar, S.: New adsorption-condensation theory for adsorption of vapors on porous activated carbons. Carbon **25**, 39–48 (1987)

Sircar, S.: Adsorbate mass transfer into porous adsorbents: a practical viewpoint. Sep. Purif. Technol. **192**, 383–400 (2018)

Sircar, S., Hufton, J.R.: Why does the linear driving force model for adsorption kinetics work? Adsorption **6**, 137–147 (2000a)

Sircar, S., Hufton, J.R.: Intraparticle adsorbate concentration profile for LDF model. AIChE J. **46**, 659–660 (2000b)

Sircar, S., Myers, A.: Gas Separation by Zeolites, Handbook of Zeolite Science and Technology. CRC, New York (2003)

Sircar, S., Rao, M.B., Golden, T.C.: Drying of gases and liquids by activated alumina. In: Dabrowski, A., Tertykh, V.A. (eds.) Adsorption on New and Modified Inorganic Sorbents. Elsevier, Amsterdsam (1996)

Son, K.N., Cmarik, G.E., Knox, J.C., Weibel, J.A., Garimella, S.V.: Measurement and prediction of the heat of adsorption and equilibrium concentration of CO_2 on zeolite 13X. J. Chem. Eng. Data **63**, 1663–1674 (2018)

Talu, O.: Measurement and analysis of mixture adsorption equilibrium in porous solids. Chem. Ing. Technol. **83**, 67–82 (2011)

Terreni, J., Trottmann, M., Franken, T., Heel, A., Borgschulte, A.: Sorption-enhanced methanol synthesis. Energy Technology **7**, 1801093 (2019)

Terreni, J., Trottmann, M., Delmelle, R., Heel, A., Trtik, P., Lehmann, E.H., Borgschulte, A.: Observing chemical reactions by time-resolved high-resolution neutron imaging. J. Phys. Chem. C **122**, 23574–23581 (2018)

van Kampen, J., Boon, J., van Berkel, F., Vente, J., van SintAnnaland, M.: Steam separation enhanced reactions: review and outlook. Chem. Eng. J. **374**, 1286–1303 (2019)

van Kampen, J., Booneveld, S., Boon, J., Vente, J., van SintAnnaland, M.: Experimental validation of pressure swing regeneration for faster cycling in sorption enhanced dimethyl ether synthesis. Chem. Commun. **56**, 13540 (2020a). https://doi.org/10.1039/D0CC06093C

van Kampen, J., Boon, J., Vente, J., van SintAnnaland, M.: Sorption enhanced dimethyl ether synthesis for high efficiency carbon conversion: modelling and cycle design. J. CO2 Util. **37**, 295–308 (2020b)

Walspurger, S., Elzinga, G.D., Dijkstra, J.W., Saric, M., Haije, W.G.: Sorption enhanced methanation for substitute natural gas production: experimental results and thermodynamic considerations. Chem. Eng. J. **242**, 379–386 (2014)

Wang, Y.: Measurements and modeling of water adsorption isotherms of zeolite linde-type A crystals. Ind. Eng. Chem. Res. **59**, 8304–8314 (2020)

Zhang, A., Zeng, W., Niemczyk, T.M., Keenan, M.R., Haaland, D.M.: Multivariate analysis of infrared spectra for monitoring and understanding the kinetics and mechanisms of adsorption processes. Appl. Spectrosc. **59**, 47–55 (2005)

Affiliations

Jasper van Kampen[1,2] · **Jurriaan Boon[1,2]** · **Martin van Sint Annaland[2]**

✉ Jasper van Kampen
jasper.vankampen@tno.nl; j.v.kampen@tue.nl

[1] Biomass and Energy Efficiency, TNO Energy Transition, P.O. Box 15, 1755 ZG Petten, The Netherlands

[2] Chemical Process Intensification, TU/e, P.O. Box 513, 5600 MB Eindhoven, The Netherlands